

## Supplementary information

# Rationally designed nickel oxide ravines@iron cobalt-hydroxides with largely enhanced capacitive performance for asymmetric supercapacitor

Libo Gao,<sup>1</sup> Ke Cao,<sup>1</sup> Hongti Zhang,<sup>1</sup> Peifeng Li,<sup>1</sup> Jian Song,<sup>1</sup> James Utama Surjadi,<sup>1</sup> Yanfang Li,<sup>2</sup> Dong Sun<sup>1</sup> and Yang Lu<sup>1,3\*</sup>

<sup>1</sup>Department of Mechanical and Biomedical Engineering, City University of Hong Kong, Kowloon, Hong Kong SAR, China

<sup>2</sup>Science and Technology on Electronic Test and Measurement Laboratory, North University of China, Taiyuan, Shanxi 030051, China

<sup>3</sup>Shenzhen Research Institute, City University of Hong Kong, Shenzhen 518057, China

\* Author to whom correspondence should be addressed;

**E-Mail:** yanglu@cityu.edu.hk

## Experimental section

### Preparation of NiO@FeCo-LDH and PGC electrode

The NiO ravines were synthesized by a facile acid corrosion following with self-oxidation methodology.<sup>1,2</sup> Briefly, pre-treated nickel foam ( $1 \times 2 \text{ cm}^2$ , electrode area  $1 \times 1 \text{ cm}^2$ ) was immersed into 3 M hydrochloric acid and kept static at  $90 \text{ }^\circ\text{C}$  for 20 min. Subsequently, the nickel foam was removed away from the solution, washed using deionized (DI) water several times, and dried naturally at room temperature for 24 h. The treated nickel foam was then directly used as the working electrode in a mixed solution of 8 mM  $\text{Co}(\text{NO}_3)_2 \cdot 6 \text{ H}_2\text{O}$  and 4 mM  $\text{FeSO}_4 \cdot 7\text{H}_2\text{O}$  mixed solution. Pt plate was used as the counter electrode and calomel electrode as the reference electrode. After electrodeposition (ED) for 15 min at -1 V, the sample, namely NiO@FeCo-LDH, was carefully taken out from the solution and washed with DI water before drying at room temperature. The mass of NiO@FeCo-LDH was measured to be  $2 \text{ mg cm}^{-2}$ . For comparison, the NiO@FeCo-LDH fabricated for  $x$  min designated as NiO@FeCo-LDH- $x$  and FeCo-LDH directly grown on nickel foam were synthesized.

The PGC electrode was synthesized via facile physical method, which is shown in Figure S1. Specifically, 20 mg of single layer graphene (XF nano, Nanjing) which has been pre-treated with nitric acid was slowly added into 10 mL of pen ink carbon nanoparticles (PICN) solution (Shanghai Factory). After leaving the solution in an ultrasonic bath for 8 h, a certain amount of CNT with average diameter of 50 nm was added. The mass ratio of CNT to graphene was fixed at 15%, which lies within the range of 10% to 20%, thus effectively avoiding dense stacking of graphene.<sup>3</sup>

Subsequently, the mixed solution was put in an ultrasonic bath again for 8 h, and then dried to evaporate the water to finally obtain the carbon powder used for the negative electrode material. To prepare the negative electrode, the synthesized carbon powder, acetylene black and poly-vinylidene fluoride (PVDF) were mixed together in a weight ratio of 8:1:1 in N-methylpyrrolidone (NMP) solution at 70 °C. The slurry is then coated on nickel foam with size of 1×2 cm<sup>2</sup>. After drying at 80 °C, the nickel foam was pressed to form a thin foil.

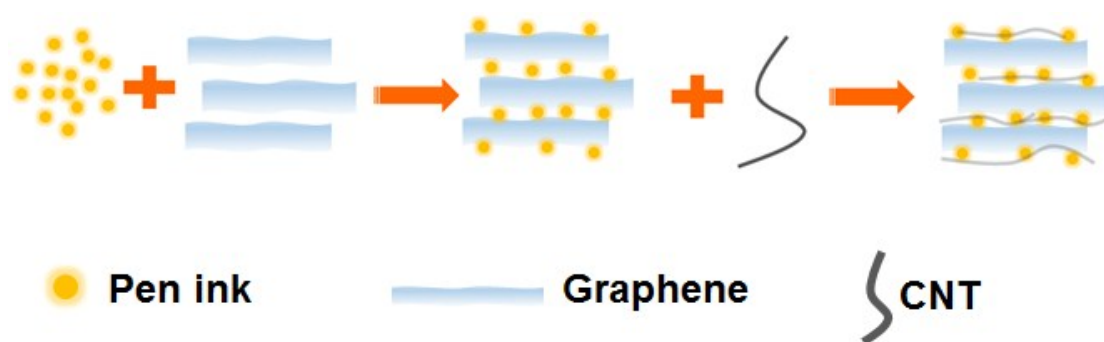


Figure S1. Schematic illustration of fabrication of the PGC.

### Materials characterization

X-ray diffraction (XRD, RigakuSmartLab) with monochromatic Cu K $\alpha$  radiation (1.5418 Å) was employed to characterize the phase structures of NiO@FeCo-LDH and PGC. The morphology and structure of the samples synthesized were analyzed using scanning electron microscope (SEM) (FEI<sup>TM</sup>, Quanta 450), transmission electron microscope (TEM) and high resolution-TEM (HRTEM) (JEOL JEM-2100F) equipped with energy dispersive X-ray spectroscopy (EDS) and selected area electron (SAED). Electrochemical working station (CHI 7660E) was employed to characterize the electrochemical performance of the samples. The N<sub>2</sub> adsorption/desorption isotherms

were tested at liquid nitrogen temperature (77 K) using a Micromeritics ASAP 2010M instrument and the specific surface area was calculated by the Brunauer Emmette Teller (BET) route. The pore size distribution was obtained using the Barrete Jonere Halenda (BJH) method.

### Electrochemical tests

In the electrochemical process, a platinum electrode (1×1 cm<sup>2</sup>) and saturated calomel electrode were regarded as the counter and reference electrode, respectively. 2 M KOH solution was used as the electrolyte. Cyclic voltammetry (CV) and galvanotactic charge-discharge (GCD) measurements were conducted in three-electrode system. The electrochemical impedance spectroscopy (EIS) was performed in the frequency of 0.01 Hz to 100 KHz. For the double electrochemical capacitance, the specific capacitance ( $C_m$ , F g<sup>-1</sup>) was calculated by the following equations:

$$C_m = \frac{I \Delta t}{m \Delta V} \quad (1)$$

For the battery-type supercapacitor and ASC, the areal capacitance ( $C_s$ , F cm<sup>-2</sup>) was calculated by using Eq 2 in GCD curves.<sup>4</sup>

$$C_s = \frac{2i_s \int V dt}{V^2 \Big|_{V_i}^{V_f}} \quad (2)$$

Where  $i_s$  (A cm<sup>-2</sup>) is the discharge current;  $\int V dt$  is the integral current area, where V is the potential with initial and final values of  $V_i$  and  $V_f$ , respectively. Similarly, the specific capacitance ( $C_m$ , F g<sup>-1</sup>) can be obtained through substituting the  $i_s$  (A cm<sup>-2</sup>) with  $i_m$  (A g<sup>-1</sup>).

Accordingly, the specific capacity Q (C m<sup>-2</sup>, C g<sup>-1</sup>), was calculated using the following

formula:

$$Q = CU \quad (3)$$

Where C is the specific (areal, mass) capacitance and U is the voltage range.

### Device fabrication

The theoretical ratio of the mass of positive electrode to negative electrode was determined in accordance with the following equation for charge balance.<sup>5</sup>

$$m_+ : m_- = \left( \int i dV/v \right)_- : \left( \int i dV/v \right)_+ \quad (4)$$

Where  $m_+(g)$  and  $m_-(g)$  is the mass of the positive electrode and negative electrode, respectively.  $i$  ( $A g^{-1}$ ) is the current density,  $V$  (V) is the potential range,  $v$  ( $mV s^{-1}$ ) is the scan rate and  $\int i/dV$  is the integral area of the cyclic voltammogram. The mass ratio in the ASC system was calculated to be approximately 0.26 according to the CV curves at  $5 mV s^{-1}$  in Figure S15. The total mass of the electrode materials for ASC was  $9.7 mg cm^{-2}$  ( $NiO@FeCo-LDH \sim 2 mg cm^{-2}$  and  $PGC \sim 7.7 mg cm^{-2}$ ). Subsequently, the two electrodes were separated by a thin PE filter membrane (thickness:  $150 \mu m$ , Japan) and combined with 2 M KOH as the electrolyte to assemble the device that finally was encapsulated with Kapton plastic film.

The specific capacitance can be obtained according to equation (1). The energy density ( $E, Wh kg^{-1}$ ) and power density ( $P, W kg^{-1}$ ) were calculated based on the following method.

$$E = 0.5C\Delta V^2 \quad (5)$$

$$P = E/\Delta t \quad (6)$$

Where  $C$  ( $F g^{-1}$ ) is the specific capacitance of the ASC, and  $m$  (g) represents the total

mass of both electrode materials.

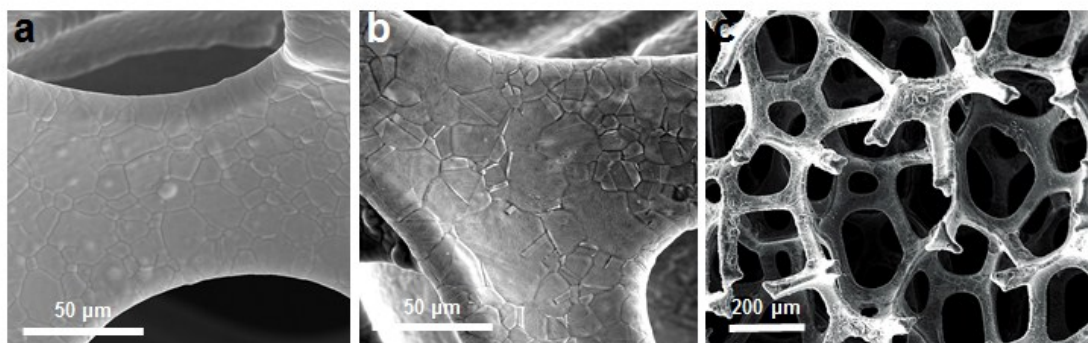


Figure S2. FESEM images of (a) is the nickel foam without acid treatment (b-c) the nickel foam fabricated with acid assistance.

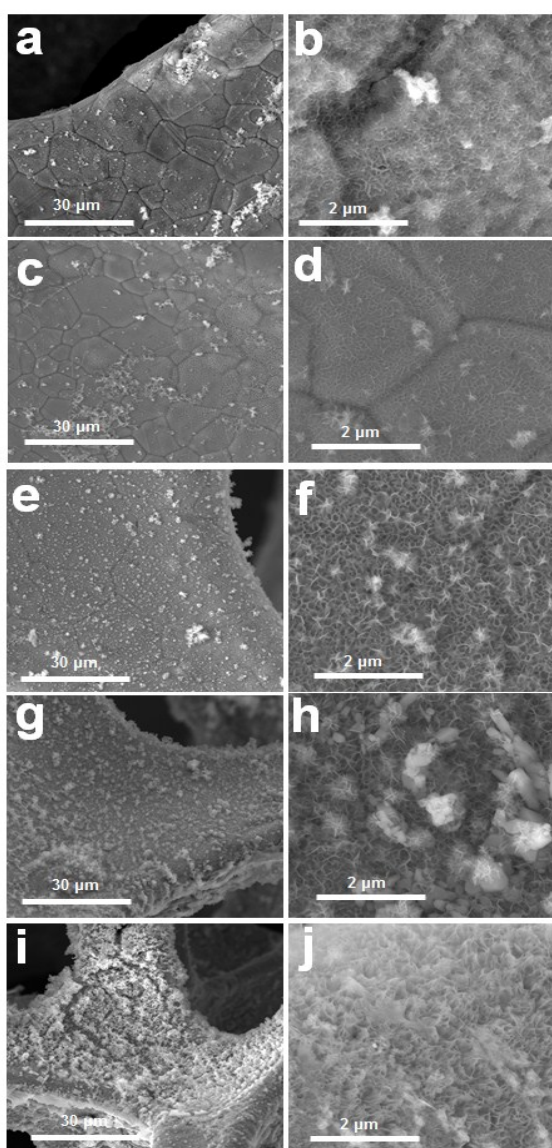


Figure S3. FESEM images of FeCo-LDH fabricated with different time: (a-b) 5 min; (c-d) 10 min; (e-f) 15 min; (g-h) 20 min; (i-j) 30 min.

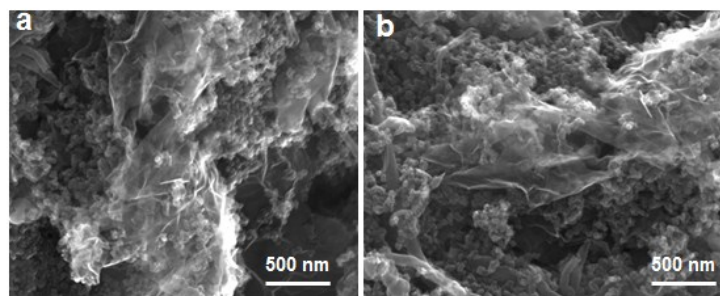


Figure S4. (a-b) FESEM images of the PGC.

Figure S5 shows the XRD patterns of the positive and negative electrode, respectively. As shown in Figure S5a, the nickel foam exhibits a strong signal behavior. After treated with acid, one yet clear signal can be indexed with NiO (JCPDS 47-1049) owing to its ultrathin feature.<sup>6,7</sup> After electrodeposition for 15 min, the NiO@FeCo-LDH exhibits the typical LDH material phase, (003), (006), (012) and (110) reflections of LDH phase ( JCPDS 51-0045) can be clearly observed.<sup>8-10</sup> Figure S4b shows the NiO@FeCo-LDH fabricated at various times, similar patterns are observed while with increasing the deposition time, the intensity of the signals become stronger, indicating the successful fabrication of the NiO@FeCo-LDH and with the enlarge time, the thickness of the FeCo-LDH become thick, which is in accordance with our SEM images. For the negative electrode, typical broad peaks are observed with carbon properties. And a strong peak can be seen which is indexed with CNT.<sup>11</sup>

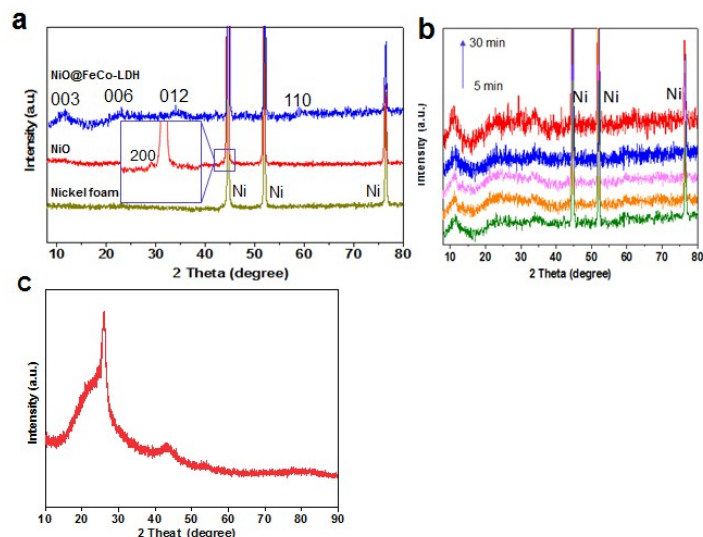


Figure S5. XRD patterns of (a) the nickel, NiO and NiO@FeCo-LDH (b) NiO@FeCo-LDH fabricated at different time (c) PGC.

As shown in Figure S6, after treated with acid, the nickel foam not only exhibits rough surface morphology, but much more oxygen element existed compared to that of the nickel foam without acid treatment. Obviously, XRD combing SEM-EDS was able to confirm the successful fabrication of NiO ravines.

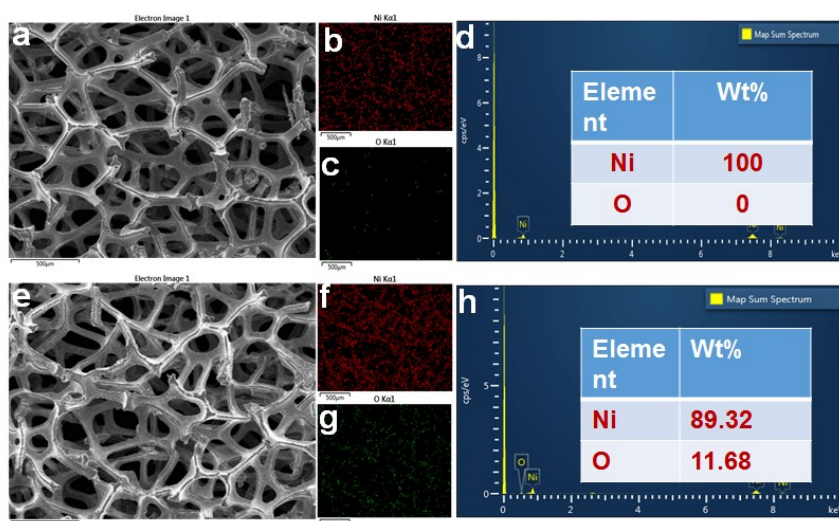


Figure S6. (a) SEM images and (b-c) corresponding EDS map and (d) element concentration of nickel foam without treatment. (e) SEM images and (f-g) corresponding EDS map and (h) element concentration of nickel foam fabricated with acid assistance.

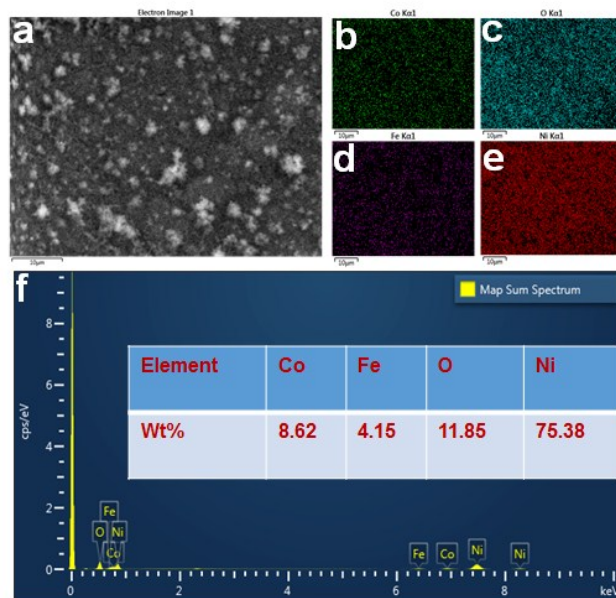


Figure S7. (a) SEM images of FeCo-LDH and (b-e) corresponding EDS map and (f) element concentration of nickel foam with acid assistance.

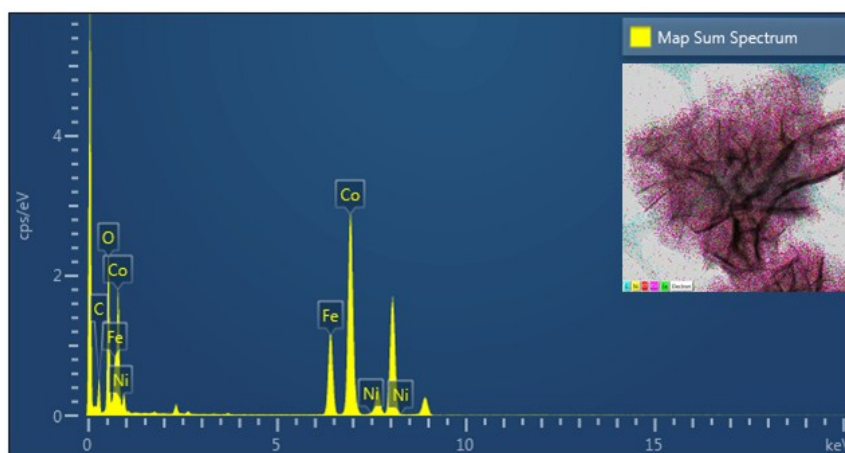


Figure S8. EDS result of the FeCo-LDH using TEM.

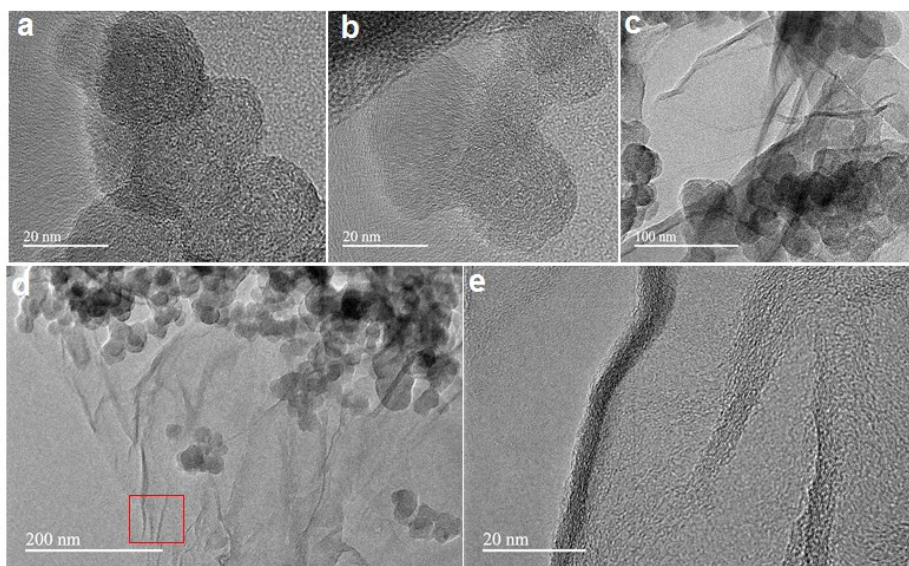


Figure S9. (a-c) TEM images of the pen ink nanoparticles. (d-e) TEM images of PGC and corresponding high resolution graphene layer.

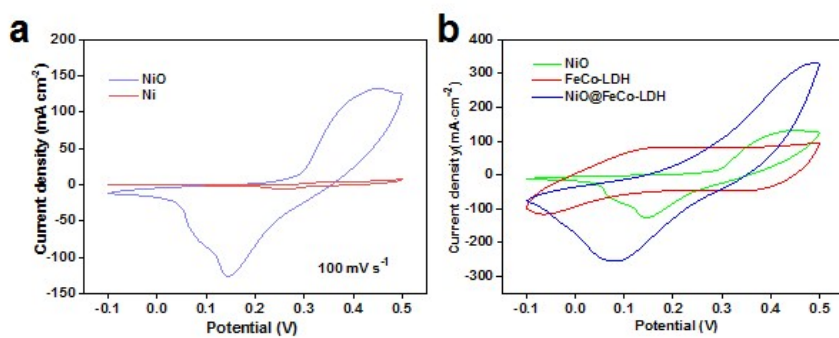


Figure S10. (a) CV curves of NiO and Ni at a scan rate of  $100 \text{ mV s}^{-1}$  (b) CV curves of NiO, FeCo-LDH and NiO@FeCo-LDH at  $100 \text{ mV s}^{-1}$ .

For the conductivity of FeCo-LDH grown on the nickel foam, the conductivity can be obtained through the IR drop (known as the voltage drop at the beginning of each discharge curve, is a measure of the internal resistance of the sample<sup>12,13</sup>). As shown in Figure S11e, the resistance of the sample is estimated to be  $0.75 \Omega \text{ cm}^{-2}$ , indicating the excellent conductivity of the FeCo-LDH.

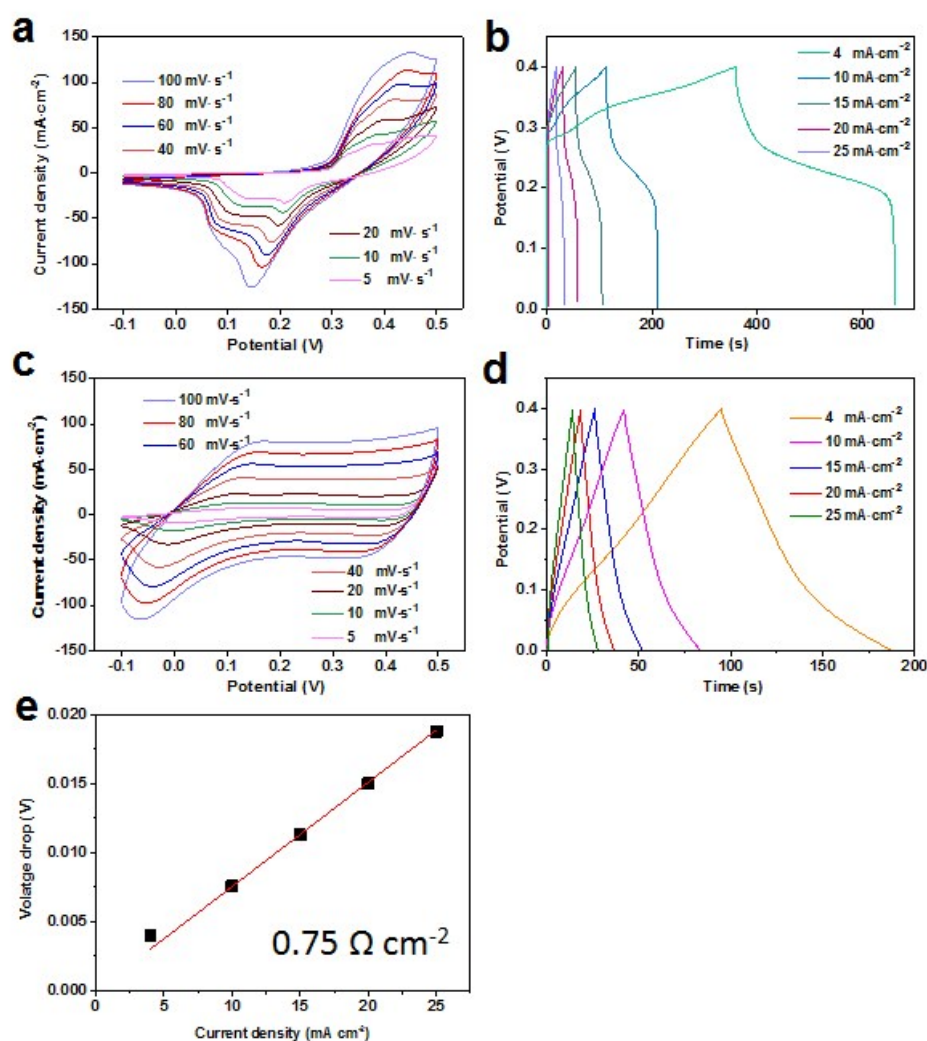


Figure S11. (a) CV curves of NiO at various scan rates. (b) GCD curves of NiO at different current densities. (c) CV curves of FeCo-LDH growing on pure nickel foam at various scan rates. (d) GCD curves of FeCo-LDH at different current densities. (e) Voltage drop change with the current densities.

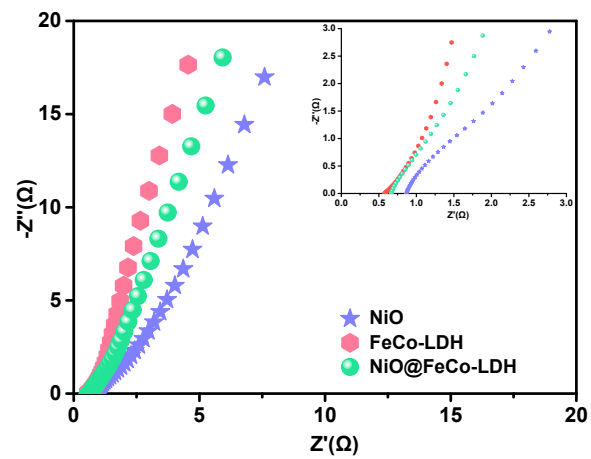


Figure S12. Nyquist plots of NiO, FeCo-LDH and NiO@FeCo-LDH.

The areal capacitance of the NiO@FeCo-15 is 4.5, 4.3, 4.13, 3.8 and 3.6 F cm<sup>-2</sup> at 4, 10, 15, 20 and 25 mA cm<sup>-2</sup>, respectively. Due to the specific mass of the electrode materials is 2 mg cm<sup>-2</sup>, correspondingly the mass specific capacitance can be calculated to be 2250, 2150, 2065, 1900 and 1800 F g<sup>-1</sup> (corresponding specific capacity of 1350, 1290, 1239, 1140 and 1080 C g<sup>-1</sup>). In Figure S13a, the CV curves of display pronounced potential disparity among oxidation and reduction peaks, corresponding to obvious polarization of the electrode materials. The larger polarization of the polarization is caused by many factors, for example, the pore size distribution, the surface morphology and crystal structures.<sup>14-16</sup> Importantly, the internal resistance (Figure S13e) of NiO@FeCo-LDH deposited at different time can be calculated through the IR drop in Figure S13b. Figure S13f shows the BET surface area and pore size distribution. The specific surface can be calculated to be 72.5 m<sup>2</sup> g<sup>-1</sup> while the pore size is mainly distributed near 2 nm, which is consisted with the TEM images.

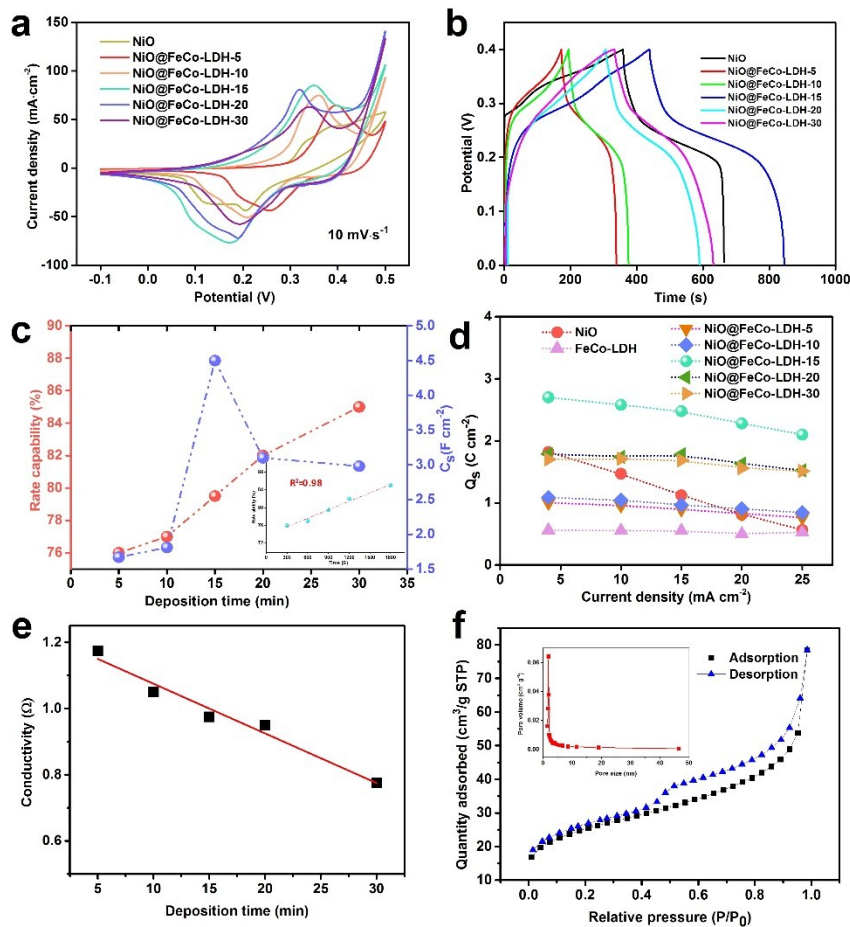


Figure S13. (a-b) CV and GCD curves of NiO@FeCo-LDH fabricated with different time, respectively. (c) Rate capability and areal capacitance with increasing the deposition time. Inset interestingly shows the rate capability improve linearly with the deposition time. (d) Areal capacitance of NiO@FeCo-LDH fabricated with different times at different current densities. (e) The conductivity of NiO@FeCo-LDH at different deposition time. (f) Nitrogen adsorption/desorption isotherms and corresponding pore size distribution (insets) of the FeCo-LDH.

As shown in Figure S14, the FeCo-LDH conserves its morphology, and no obvious swell and

collapse of the FeCo-LDH nanosheets were observed, suggesting its good mechanical behavior in resisting the electrolyte insertion/deinsertion during charge/discharge process. Importantly, almost 93% capacitance retention was obtained even after 3000 cycles of CV test at  $100 \text{ mV s}^{-1}$ , demonstrating its excellent stability.

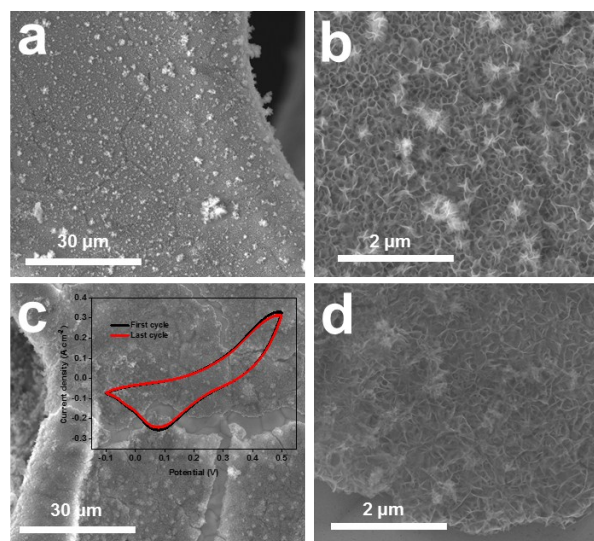


Figure S14. (a-b) SEM images of the NiO@FeCo-LDH before cycling test. (c-d) SEM images of the NiO@FeCo-LDH after cycling for 3000 times. Inset is corresponding CV curves of the first and last cycle.

The specific capacitance of the PGC is calculated to be 171.1, 166.4, 150, 136.9, and  $110.6 \text{ F g}^{-1}$ , at corresponding current densities of 1 to  $4 \text{ A g}^{-1}$ .

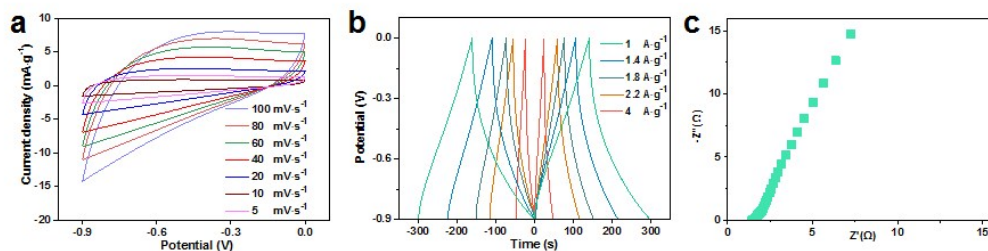


Figure S15. (a) CV curves (b) GCD curves and (c) Nyquist plots of PGC.

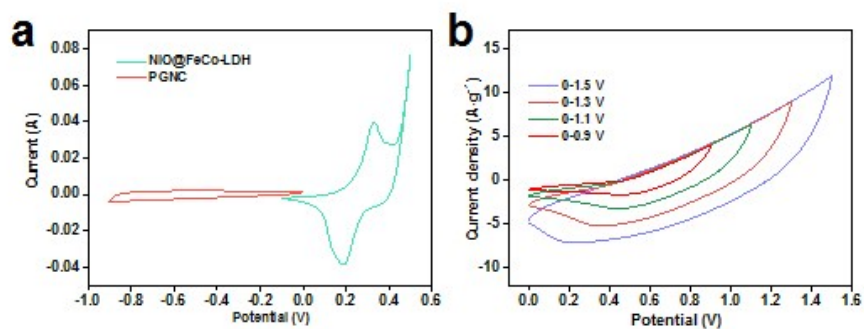


Figure S16. (a) CV curves of NiO@FeCo-LDH and PGC at a scan rate of 5 mV s<sup>-1</sup>. (b) CV curves of the ASC at different operating potential window at a scan rate of 60 mV s<sup>-1</sup>.

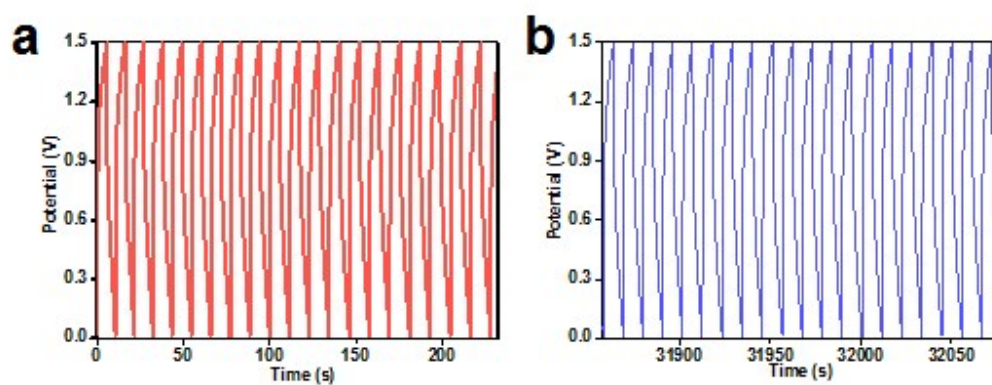


Figure S17. The initial (a) and last (b) several cycles of the ASC.

Table S1. Comparison of the capacitive performance of NiO@FeCo-LDH with other LDH

<b>Electrode materials</b>	<b>Capacitance</b>	<b>Rate capability</b>	<b>Reference</b>
MnO <sub>2</sub> @NF/NiFe-LDH	4.3 F cm <sup>-2</sup> at 5 mA cm <sup>-2</sup>	42% (From 5 to 20 mA cm <sup>-2</sup> )	17
CoNi-LDH	1.62 F cm <sup>-2</sup> at 1 mA cm <sup>-2</sup>	75.8% (From 1 to 30 mA cm <sup>-2</sup> )	18
NiMn-LDH	1635 F g <sup>-1</sup> at 1A g <sup>-1</sup>	71% (from 1 to 10 Ag <sup>-1</sup> )	19
NiCo-LDH/carbon nanofoam	1.52 C cm <sup>-2</sup> /2.03 F cm <sup>-2</sup> at 2.1 mA cm <sup>-2</sup>	87% (from 2 to 7 mA cm <sup>-2</sup> )	20
NiCo-LDH/Graphene	2.08 F cm <sup>-2</sup> at 2.5 mA cm <sup>-2</sup>	60% (from 2.5 to 50 mA cm <sup>-2</sup> )	21
CoAl LDH@Ni(OH) <sub>2</sub>	2.08 F cm <sup>-2</sup> at 5 mA cm <sup>-2</sup>	73% (from 5 to 20mA cm <sup>-2</sup> )	22
NiO@FeCo-LDH	2.7 C cm <sup>-2</sup> /4.5 F cm <sup>-2</sup> at 4 mA cm <sup>-2</sup>	80% (from 4 to 25 mA cm <sup>-2</sup> )	<b>Our work</b>

## References

- 1 X. Liu, G. Chen, H. Guan, C. Dong, X. Xiao and Y. Wang, *Electrochim. Acta*, 2016, **189**, 83–92.
- 2 M. Yu, W. Wang, C. Li, T. Zhai, X. Lu and Y. Tong, *NPG Asia Mater.*, 2014, **6**, e129.
- 3 J. P. C. Trigueiro, R. L. Lavall and G. G. Silva, *Electrochim. Acta*, 2016, **187**, 312–322.
- 4 L.-Q. Mai, A. Minhas-Khan, X. Tian, K. M. Hercule, Y.-L. Zhao, X. Lin and X. Xu, *Nat. Commun.*, 2013, **4**, 2923.
- 5 B. Zhao, D. Chen, X. Xiong, B. Song, R. Hu, Q. Zhang, B. H. Rainwater, G. H. Waller, D. Zhen, Y. Ding, Y. Chen, C. Qu, D. Dang, C.-P. Wong and M. Liu, *Energy Storage Mater.*, 2017, **7**, 32–39.
- 6 S. . Wu, K. S. . Hui, K. N. . Hui and K. H. . d Kim, *J. Mater. Chem. A*, 2016, **4**, 9113–9123.
- 7 Y. H. Ko, G. Nagaraju and J. S. Yu, *Nanoscale*, 2015, **7**, 2735–2742.
- 8 K. Ma, F. Liu, M. Zhang, X. Zhang and J. P. Cheng, *Electrochim. Acta*, 2017, **225**, 425–434.
- 9 Z. Li, M. Shao, L. Zhou, R. Zhang, C. Zhang, J. Han, M. Wei, D. G. Evans and X. Duan, *Nano Energy*, 2016, **20**, 294–304.
- 10 P. Sun, R. Lin, Z. Wang, M. Qiu, Z. Chai, B. Zhang, H. Meng, S. Tan, C. Zhao and W. Mai, *Nano Energy*, 2016, **31**, 432–440.
- 11 Z. Sun, Z. Liu, B. Han, S. Miao, Z. Miao and G. An, *J. Colloid Interface Sci.*, 2006, **304**, 323–328.
- 12 Z. Ren, J. Li, Y. Ren, S. Wang, Y. Qiu and J. Yu, *Sci. Rep.*, 2016, **6**, 20021.
- 13 M. F. El-Kady and R. B. Kaner, *Nat. Commun.*, 2013, **4**, 1475.
- 14 L. Ye, L. Zhao, H. Zhang, P. Zan, S. Gen, W. Shi, B. Han, H. Sun, X. Yang and T. Xu, *J. Mater. Chem. A*, 2017, **5**, 1603–1613.
- 15 J. Liu, M. Chen, L. Zhang, J. Jiang, J. Yan, Y. Huang, J. Lin, H. J. Fan and Z. X. Shen, *Nano Lett.*, 2014, **14**, 7180–7187.
- 16 X. He, Q. Liu, J. Liu, R. Li, H. Zhang, R. Chen and J. Wang, *Chem. Eng. J.*, 2017, **325**, 134–143.
- 17 M. Li, M. Zhou, Z. Q. Wen and Y. X. Zhang, *J. Energy Storage*, 2017, **11**, 242–248.

- 18 J. Wu, W. Liu, Y. Wu, T. Wei, D. Geng, J. Mei, H. Liu, W. Lau and L. Liu, *Electrochim. Acta*, 2016, **203**, 21–29.
- 19 M. Li, J. P. Cheng, J. Wang, F. Liu and X. B. Zhang, *Electrochim. Acta*, 2016, **206**, 108–115.
- 20 T. Nguyen, M. Boudard and M. Joa, *Energy*, 2017, **126**, 208–216.
- 21 X. Bai, Q. Liu, H. Zhang, J. Liu, Z. Li and X. Jing, *Electrochim. Acta*, 2016, **215**, 492–499.
- 22 W. Hong, J. Wang, L. Niu, J. Sun, P. Gong and S. Yang, *J. Alloy. Compd.*, 2014, **608**, 297–303.